Laser-induced photothermoacoustic pressure-wave pulses in a polystyrene well and water system used for photomechanical drug delivery

Andreas Mandelis and Natalie Baddour

Center for Advanced Diffusion-Wave Technologies, Department of Mechanical and Industrial Engineering, University of Toronto, Toronto, Ontario M5S 3G8, Canada

Ying Cai and Richard G. Walmsley

Norwood Abbey Limited, 63 Wells Road, Chelsea Heights, Victoria 3196, Australia

Received January 31, 2004; revised manuscript received July 15, 2004; accepted November 29, 2004

A linear time-domain thermoelastic (photothermoacoustic) theory of a composite solid–liquid geometry has been developed. The theory includes multiple interreflections at all interfaces, acoustic diffraction and viscosity effects, and natural mixed, rigid, and free boundary conditions at the solid surface where laser-pulse incidence occurs (air–polystyrene interface). The theory was applied to experimental pressure-wave pulses from a Nd:YAG laser in a polystyrene well target and water system used for photomechanical drug delivery studies. Good fits of the linear theory to tripolar experimental pressure waveforms were possible at laser-pulse irradiances $\leqslant$100 MW/cm^2, especially at distances $\leqslant$5 mm from the solid–fluid interface. It was further determined from the combined theoretical and experimental approach that the onset of significant hydrodynamic nonlinearity in the water appears for laser-pulse irradiances in the 165-MW/cm^2 range, especially at axial distances $z \sim 8$ mm, as expected theoretically from the laser-ablation-induced nonlinearity of stress-wave propagation in the solid–water system.

OCIS codes: 170.7170, 170.7180.

1. INTRODUCTION

The field of drug delivery and cell permeabilization with laser-induced stress waves has witnessed a rapid development in recent years, with several research groups reporting various levels of success in generating reliable and reproducible cell membrane permeabilization results.[1–4] Much attention has been paid to the experimenter's ability to control the rising edge of the laser photoacoustic stress pulse in the fluid (water) as a tool to control cell permeabilization.[1,2] It is broadly believed that nonlinear photoacoustic waves must be generated in water to induce cell permeabilization. A review of the literature, however, has revealed that photoacoustic pulse shapes in cell-loaded wells filled with water may exhibit a wide range of linear and nonlinear behavior with poor understanding of the parameters that lead to a particular response. Reported results are sometimes consistent with thermoelastic wave propagation[3] and sometimes with nonlinear shock waves.[4] This may be related to the fact that there appears to be no full understanding of the effects and ranges of the various experimental control parameters that lead to nonlinearity. This, in turn, compromises the reproducibility of the photomechanical experiment and the predictability and optimization of the cell permeabilization and drug delivery yield. Reflecting the same situation, theoretical photoacoustic treatments of the pulse generation and propagation mechanism in the fluid vary widely, ranging among linear, fully nonlinear, and quasi-linear approaches, even within the same research group. To control the photomechanical pulse behavior and to obtain consistently reproducible waveforms among the different groups, a theoretical treatment of the linear thermoelastic mechanism[5] and an understanding of its transition to nonlinear stress-wave generation should be considered. The major measurable difference between the nonlinear impulse response and the linear thermoelastic response is the crucial steepening of the fluid pressure-pulse rising edge with increasing laser irradiance.[6]

In this paper a first step in this direction, the problem of linear photomechanical pressure-pulse generation in water, the fluid of choice in many cell membrane permeabilization studies,[1–4] is formulated. A laser pulse incident on the outer surface of a standard solid black polystyrene well target in a conventional configuration for cell permeabilization[1–4] is considered as the source of a photothermoacoustic (PTA) pulse in the solid. Coupled small-amplitude (linear) wave equations are solved in the solid and fluid, and the resulting predictions are compared with experimental data obtained with a variable-fluence pulsed Nd:YAG laser and commercially available polystyrene wells filled with water. Unlike the two boundary-condition modes always used separately in the laser photoacoustics literature[3,7] (which were unable to match our experimental results), following excitation by an incident single-shot laser pulse, the present one-dimensional model introduces natural mixed (free and rigid) boundary conditions and accounts for acoustic diffraction and fluid

0740-3224/05/051024-13/$15.00

viscosity effects, as well as for multiple acoustic reflections at the air–solid and solid–fluid interfaces. A study of the onset of deviations between the linear theory and the experimental data is used as a practical criterion to determine the threshold laser irradiance required for the generation of large-amplitude photoacoustic waves in the fluid and the transition to nonlinearity.

2. THEORY OF PHOTOTHERMOACOUSTIC LASER PULSES IN FLUIDS

A. Coupled Photothermoacoustic Boundary-Value Problems

In a nonviscous fluid undergoing small acoustic perturbations affecting the density up to the linear term,

$$\rho_f(\mathbf{r},t) = \rho_{f0} + \rho_1(\mathbf{r},t), \tag{1}$$

where subscript 0 indicates equilibrium values. Introducing a scalar velocity potential

$$\mathbf{V}(\mathbf{r},t) = \nabla \Psi_f(\mathbf{r},t), \tag{2}$$

it can be shown that $\Psi_f(\mathbf{r},t)$ $(\mathrm{m}^2\,\mathrm{s}^{-1})$ satisfies (Ref. 7, Chap. 2)

$$\frac{\partial^2 \Psi_f(\mathbf{r},t)}{\partial t^2} - {c_{f0}}^2 \nabla^2 \Psi_f(\mathbf{r},t) = -\left(\frac{T_{f0}{c_{f0}}^2\beta}{C_P}\right)\frac{\partial S_1(\mathbf{r},t)}{\partial t}. \tag{3}$$

Also introducing the heat conduction equation and the adiabatic medium ratio of specific heats, $\gamma = C_P/C_v$, such that $\gamma \simeq 1$ for condensed media (Ref. 7, Chap. 2), leading to

$$\gamma - 1 = \frac{T_{f0}{c_{f0}}^2\beta^2}{C_P} \ll 1,$$

an equation for PTA wave generation in a nonviscous heat-conducting fluid can be written as

$$\frac{\partial^2 \Psi_f(\mathbf{r},t)}{\partial t^2} - {c_{f0}}^2 \nabla^2 \Psi_f(\mathbf{r},t) = -\frac{{c_{f0}}^2\beta}{\rho_{f0}C_P}\nabla \cdot \mathbf{Q}(\mathbf{r},t), \tag{4}$$

where β (K^{-1}) is the coefficient of volume v, expansion $\beta = v^{-1}(\,\mathrm{d}v/\mathrm{d}T|_P)$, c_{f0} is the equilibrium value of the speed of sound in the fluid within the linear regime, and C_P is the specific heat at constant pressure. $\mathbf{Q}(\mathbf{r},t)$ is the directional source in the fluid. In this formalism $\mathbf{Q}=0$ as the source for the acoustic disturbance in the fluid originates in the supporting optically absorbing solid in the form of a PTA pulse. The small-amplitude pressure rise in the fluid is related to the potential Ψ_f by[8]

$$P_f(\mathbf{r},t) = -\rho_{f0}\frac{\partial}{\partial t}\Psi_f(\mathbf{r},t), \tag{5}$$

where the pressure increase $P_f(\mathbf{r},t)$ is assumed to involve only the PTA pressure rise. The electrostrictive component of the pressure is ignored.[9]

The geometry used in our experiments employed a large laser beam ($\geqslant$5 mm) and thus corresponds to the one-dimensional limit of Eq. (4). Figure 1 describes the three effective coupled layers: The ambient gas (air) is semi-infinite and occupies the spatial region $-\infty < z \leqslant -L$. It has density ρ_a and speed of sound c_a. The solid of thickness L occupies the domain $-L \leqslant z \leqslant 0$ and has properties of density ρ_s, speed of sound c_s, specific heat at constant pressure C_{Ps}, optical absorption coefficient at the laser-pulse wavelength μ_s, bulk modulus K_s, and isobaric volume expansion coefficient β_s. The fluid occupies the half-space $0 \leqslant z < \infty$. The reason that we do not consider the finite thickness of the fluid layer is that in our experiments no reflections from the water–air interface (expected to be inverted pulses[10]) were observed. This simplifies the solution, but the finite dimensions of the fluid can be readily incorporated in the theory. The coupled-wave equations in the solid and fluid are most conveniently dealt with by introducing in the solid a particle–molecule displacement potential $\Phi_s(\mathbf{r},t)$, which is related to the displacement vector $\mathbf{U_s}(\mathbf{r},t)$ by[11,12]

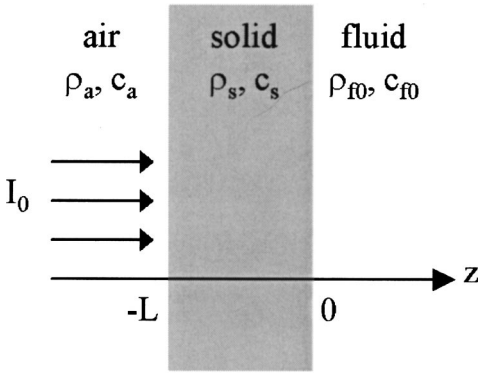

Fig. 1. One-dimensional cross-sectional geometry of the model showing the direction of the incident laser pulse.

$$\mathbf{U_s}(\mathbf{r},t) = \nabla \Phi_s(\mathbf{r},t). \tag{6}$$

Only longitudinal waves are assumed to propagate in a thin isotropic solid because of laser PTA excitation by a large-spot-size laser beam. As a result, $\nabla \times \mathbf{U_s}(\mathbf{r},t) = 0$, and the displacement potential satisfies the wave equation

$$\nabla^2 \Phi_s(\mathbf{r},t) - \frac{1}{{c_s}^2}\frac{\partial^2}{\partial t^2}\Phi_s(\mathbf{r},t) = \left(\frac{K_s\beta_s}{\rho_s{c_s}^2}\right)\Theta_s(\mathbf{r},t), \tag{7}$$

where $\Theta_s(\mathbf{r},t)$ is the temperature increase above the ambient (equilibrium) value. The thermoelastic pressure in the solid is determined by[11]

$$P_s(\mathbf{r},t) = -\rho_s\frac{\partial^2}{\partial t^2}\Phi_s(\mathbf{r},t). \tag{8}$$

In the remainder of the theoretical development, the one-dimensional version of the wave equations is used for the experimental case of a large and (assumed) uniform laser beam source. Analytical solutions of the coupled PTA problem in one and higher dimensions in the form of spectral integrals can be obtained by converting the time-domain equations to their frequency-domain counterparts through Fourier transformations (FTs). In the solid layer the equation for the FT of the one-dimensional displacement potential

$$\phi_s(z,\omega) = \frac{1}{2\pi}\int_{-\infty}^{\infty} \Phi_s(z,t)\exp(-i\omega t)\mathrm{d}t \tag{9}$$

is the Helmholtz equation,

$$\frac{\mathrm{d}^2}{\mathrm{d}z^2}\phi_s(z,\omega) + {k_s}^2\phi_s(z,\omega) = \left(\frac{K_s\beta_s}{\rho_s {c_s}^2}\right)\vartheta_s(z,\omega), \quad -L \leqslant z \leqslant 0, \tag{10}$$

where $k_s = \omega/c_s$ and $\vartheta_s(z,\omega)$ is the FT of the temperature profile $\Theta_s(z,t)$ [Eq. (7)]. The FT of the heat conduction equation in the solid following a laser pulse is the thermal-wave equation

$$\frac{\mathrm{d}^2}{\mathrm{d}z^2}\vartheta_s(z,\omega) - \left(\frac{i\omega}{\alpha_s}\right)\vartheta_s(z,\omega) = -\frac{1}{\lambda_s}H(z,\omega), \tag{11}$$

where α_s and λ_s are, respectively, the thermal diffusivity and conductivity of the solid medium. The spectral component $H(z,\omega)$ of the source term, at any angular frequency ω of the thermal source, is given by

$$H(z,\omega) = \mu_s I_0 \exp[-\mu_s(L+z) + i\omega t]. \tag{12}$$

Here I_0 is the laser irradiance. For a short laser pulse, the diffusion term in Eq. (11) can be neglected and the FT of the temperature field can be readily calculated as

$$\vartheta_s(z,\omega) = -\left(\frac{iI_0\mu_s}{\omega\rho_s C_{sP}}\right)\exp[-\mu_s(L+z)], \tag{13}$$

where the modulation factor $\exp(i\omega t)$ will henceforth be omitted. This expression is the driving force of the PTA wave in Eq. (10). The general solution to that equation is

$$\phi_s(z,\omega) = A_{s1}\exp(ik_s z) + A_{s2}\exp(-ik_s z) + D_s\exp[-\mu_s(L+z)], \tag{14a}$$

where A_{s1} and A_{s2} are integration constants to be determined and D_s is defined as follows:

$$D_s = -\frac{iK_s\beta_s I_0\mu_s}{{\rho_s}^2{c_s}^2 C_{sP}\omega({\mu_s}^2 + {k_s}^2)}. \tag{14b}$$

A similar treatment of the fluid in terms of the FT of the velocity potential $\psi_f(z,\omega)$, assuming a nonviscous fluid with no direct internal PTA source, yields the FT of Eq. (4):

$$\frac{\mathrm{d}^2}{\mathrm{d}z^2}\psi_f(z,\omega) + {k_{0f}}^2\psi_f(z,\omega) = 0, \quad 0 \leqslant z \leqslant \infty. \tag{15}$$

Here $k_{0f} = \omega/c_{0f}$ is the acoustic wave number in the fluid for small-amplitude (linear) acoustic perturbations. The (bounded) general solution of Eq. (15) is

$$\psi_f(z,\omega) = C_1\exp(-ik_{0f}z). \tag{16}$$

In the fluid (air) region of the laser incidence, $z \leqslant -L$, the FT of the PTA field is an equation similar to Eq. (15) with a general solution

$$\psi_a(z,\omega) = C_2\exp[ik_a(z+L)]. \tag{17}$$

The constants $(A_{s1}, A_{s2}, C_1, C_2)$ in Eqs. (14)–(17) can be determined through the boundary conditions at the two interfaces $z=0$ and $-L$. For an isotropic solid, the thermoelastic stress tensor σ_{ij} (Refs. 9 and 11) becomes uniaxial:

$$\sigma_{zz}(z,t) = \rho_s {c_s}^2 u_{zz}(z,t) - K_s\beta_s\Theta_s(z,t). \tag{18}$$

Equation (18) is strictly valid in the adiabatic sound propagation regime, i.e., for frequencies[11] $\omega \ll \omega_\lambda \equiv {c_s}^2\rho_s C_{sP}/\lambda_s$. If the strain tensor is written in terms of the displacement potential,

$$u_{zz}(z,t) = \frac{\partial^2}{\partial z^2}\Phi_s(z,t), \tag{19}$$

the equations for continuity of the force per unit area (pressure) at the solid–fluid and solid–gas interfaces can be deduced from Eq. (18) and their FTs can be taken as

$$\rho_s {c_s}^2\frac{\mathrm{d}^2}{\mathrm{d}z^2}\phi(0,\omega) - K_s\beta_s\vartheta_s(0,\omega) = -p_f(0,\omega) = i\rho_{f0}\omega\psi_f(0,\omega), \tag{20a}$$

$$\begin{aligned}\rho_s {c_s}^2\frac{d^2}{dz^2}\phi_s(-L,\omega) - K_s\beta_s\vartheta_s(-L,\omega) &= p_a(-L,\omega)\\ &= i\rho_a\omega\psi_a(-L,\omega),\end{aligned} \tag{20b}$$

where $p_j(z,\omega)$ is the FT of $P_j(z,t)$. Given our use of different elastic potentials in the solid and the fluid, the other continuity condition at the two interfaces is taken to be that of velocities (and accelerations) instead of displacements:

$$V_s(z,t) = \frac{\partial}{\partial t}U_s(z,t) = \frac{\partial^2}{\partial z\partial t}\Phi_s(z,t) \Rightarrow v_s(z,\omega) = i\omega\frac{d}{dz}\phi_s(z,\omega). \tag{21}$$

Upon equating the velocity FTs across the interfaces $z=0$ and $-L$, we obtain the additional boundary conditions

$$i\omega\frac{\mathrm{d}}{dz}\phi_s(0,\omega) = \frac{\mathrm{d}}{\mathrm{d}z}\psi_f(0,\omega), \tag{22a}$$

$$i\omega\frac{\mathrm{d}}{\mathrm{d}z}\phi_s(-L,\omega) = \frac{\mathrm{d}}{\mathrm{d}z}\psi_a(-L,\omega). \tag{22b}$$

Continuity of the accelerations across the same interfaces leads to a pair of boundary conditions identical to Eqs. (22). Equations (20a), (20b), (22a), and (22b) constitute the entire set of the Fourier-transformed boundary conditions that must be used to determine the integration constants $(A_{s1}, A_{s2}, C_1, C_2)$. After some algebra and with the simplification $\exp(-\mu_s L) = 0$ for optically opaque solid materials as in the case of our experiments (black polystyrene wells), the coefficients A_{s1}, A_{s2} of the PTA frequency element in the fluid can be determined:

$$A_{s2} = \frac{I_0 K_s \beta_s \mu_s [\mu_s c_a(\rho_a/\rho_s) + i\omega]\exp(-ik_s L)}{\rho_s{}^2 c_s{}^2 C_{sP} \omega^2 (\mu_s{}^2 + k_s{}^2)(1 + r_{as})[1 - R_{fs} R_{as} \exp(-2ik_s L)]}, \tag{23a}$$

$$A_{s1} = -R_{fs} A_{s2}, \tag{23b}$$

where

$$r_{ij} = \frac{\rho_i c_i}{\rho_j c_j} \tag{24}$$

is the acoustic impedance at the interface (i,j) representing energy flow between adjacent media and

$$R_{ij} = \frac{1 - r_{ij}}{1 + r_{ij}} \tag{25}$$

is the reflectance of the acoustic interface. Because of Eq. (5) and expressing C_1 in terms of A_{s2} by the boundary conditions, we can write the FT of the pressure wave as

$$p_f(z,\omega) = \rho_s \omega^2 T_{fs} A_{s2}(\omega)\exp(-ik_{0f} z), \tag{26}$$

where

$$T_{ij} = \frac{2}{1 + r_{ij}} \tag{27}$$

is the acoustic transmission coefficient at the interface (i,j). Specifically, T_{fs} represents the fraction of PTA wave energy in the solid transmitted into the fluid. To link the FT of the PTA pressure wave in the fluid to existing theoretical formalisms and make its physical interpretation more transparent, use of Eq. (23a) in Eq. (26) and expansion of the denominator yields

$$p_f(z,\omega) = \frac{I_0 K_s T_{fs}}{c_s(1 + r_{as})}[r_{as}\Gamma_{Rs}(\omega) + \Gamma_{Fs}(\omega)] \times \exp(-ik_{0f} z)\sum_{n=0}^{\infty} (R_{fs} R_{as})^n \exp[-i(2n+1)k_s L]. \tag{28}$$

In Eq. (28) the summation represents infinite interreflections of the PTA wave inside the solid layer. With each successive reflection from one of the solid boundaries, the fraction of reflected energy decreases by the product $R_{fs}R_{as}$ of the interface reflectances. The coefficients $\Gamma_{Rs}(\omega)$ and $\Gamma_{Fs}(\omega)$ are defined as follows:

$$\Gamma_{Rs}(\omega) \equiv \frac{\beta_s}{\rho_s C_{sP}}\left(\frac{\mu_s{}^2}{\mu_s{}^2 + k_s{}^2}\right), \tag{29}$$

$$\Gamma_{Fs}(\omega) \equiv \frac{i\beta_s}{\rho_s C_{sP}}\left(\frac{\mu_s k_s}{\mu_s{}^2 + k_s{}^2}\right), \tag{30}$$

where $\Gamma_{Rs}(\omega)$ and $\Gamma_{Fs}(\omega)$ are air–solid interface factors known as the transfer functions for rigid and free boundaries, respectively.[7,13] The linear combination of these factors, the former factor weighed by the acoustic impedance at the air–solid interface, indicates the effects of natural mixed boundary conditions at the air–solid interface. Unlike treatments in the literature where either rigid (subscript R) or free (subscript F) boundary conditions have been imposed arbitrarily,[7,13,14] the present approach has formulated a natural combination of the two limiting cases. The combination of these two terms in Eq. (28) is consistent with the following physical mechanism: If the acoustic (thermoelastic) transit time across a depth equal to the optical absorption depth $\mu_s{}^{-1}$ in the solid is short compared to the period corresponding to the particular frequency component of the external force, $T_\omega = 2\pi/\omega$, i.e.,

$$\tau_{\mu_s} = \frac{1}{\mu_s[c_s(\rho_a/\rho_s)]} \ll T_\omega, \tag{31}$$

where $c_s(\rho_a/\rho_s)$ is the speed of sound in the solid modified by the discontinuity in material densities at the solid–air boundary where absorption occurs, then the solid behaves like a rigid body. The acoustic energy is released before the photothermoelastically excited molecules of the solid can move to perform forced oscillation at the particular frequency. In this case the free boundary component $\Gamma_{Fs}(\omega)$ given by Eq. (30) is negligible compared with the rigid component $r_{as}\Gamma_{Rs}(\omega)$. At the other extreme, if $\tau_{\mu_s} \gg T_\omega$, the forced oscillation occurs well before the acoustic energy from within the optical absorption depth is fully released or propagated. In this (optically translucent or transparent) case the solid is under motion while the wave evolves. Therefore it behaves like a freely moving body, and the gas–solid term $r_{as}\Gamma_{Rs}(\omega)$ is negligible compared with $\Gamma_{Fs}(\omega)$. For the discussion that follows, it is convenient to redefine the two superposition components of the pressure wave in the fluid [Eq. (28)].

$$p_f(z,\omega) \equiv p_f^{(R)}(z,\omega) + p_f^{(F)}(z,\omega) \tag{32}$$

as due to rigid and free boundary conditions, respectively, where

$$p_f^{(R)}(z,\omega) = \frac{I_0 K_s T_{fs}}{c_s}\left(\frac{r_{as}}{1 + r_{as}}\right) f_s(L,\omega)\Gamma_{Rs}(\omega)\exp(-ik_{0f} z), \tag{33a}$$

$$p_f^{(F)}(z,\omega) = \frac{I_0 K_s T_{fs}}{c_s}\left(\frac{1}{1 + r_{as}}\right) f_s(L,\omega)\Gamma_{Fs}(\omega)\exp(-ik_{0f} z). \tag{33b}$$

These are the FTs of the pressure waves under fully rigid and free boundary conditions, respectively. Here

$$f_s(L,\omega) \equiv \sum_{n=0}^{\infty} (R_{fs} R_{as})^n \exp[-i(2n+1)k_s L] \tag{34}$$

is an acoustic transfer function in the solid of finite thickness L where an acoustic field of unit intensity is undergoing infinite interreflections.

B. Diffraction Effects in the Fluid

Next, the transfer function in the brackets of Eq. (28) must be modified to allow for diffraction in the fluid. This is a way of introducing three-dimensional effects into a one-dimensional formalism. Taking into account the

Gaussian nature of the laser beam of finite spot size W incident on the solid, the Fourier component of the laser-pulse profile can be modified:

$$I(x,y,z;\omega) = I_0 \exp[-(r/W)^2 - \mu_s(z+L) + i\omega t]. \quad (35)$$

The acoustic wave in the fluid will cross the boundary from the near field to the far field at distances such that $z \gg L_D$, where the diffraction length in the fluid at angular frequency ω is

$$L_D(\omega) = \frac{\omega W^2}{2c_{f0}}. \quad (36)$$

It can be shown that diffraction effects in the fluid can be accommodated in the one-dimensional theory if the transfer functions $\Gamma_{Rs}(\omega)$ and $\Gamma_{Fs}(\omega)$ are modified as follows[7]:

$$\Gamma_{Rs,Fs}(\omega) \to \Gamma^{(D)}_{Rs,Fs}(r,\omega) = \frac{\Gamma_{Rs,Fs}(\omega)}{1 - i(z/L_D)} \exp\left[-\frac{r^2}{1 - i(z/L_D)}\right]. \quad (37)$$

The origin of the diffraction term above rests with the extent to which the optically generated acoustic waves remain plane across the beam diameter. As in wave optics, the acoustic wave field of a circular laser beam of constant diameter and intensity exhibits near-field (Fresnel) and far-field (Fraunhofer) structure.[15] Diffraction determines the transition of the PTA field from the near-field to the far-field configuration with a given laser beam spot size and a realistic Gaussian transverse profile. Diffraction effects become pronounced when the detection distance is large compared to the spot size. For detection of the PTA pressure wave on the axis of symmetry (e.g., by a sensitive hydrophone), one only needs to consider $\Gamma^{(D)}_{Rs,Fs}(0,\omega)$. In this case, a diffraction transfer function is introduced for convenience:

$$\Gamma^{(D)}_{Rs,Fs}(0,\omega) = \Gamma_{Rs,Fs}(\omega) g_f(\omega), \quad (38)$$

where

$$g_f(\omega,z) = \frac{1}{1 - i(\Omega_f/\omega)}, \quad \Omega_f(z) \equiv \frac{2c_{f0}z}{W^2}. \quad (39)$$

Equation (38) is valid for on-axis detection only and has been satisfied in our experiments upon careful positioning of a hydrophone along the symmetry axis of the polystyrene well. $g_f(\omega)$ indicates lateral spreading and curvature shaping of the otherwise plane wave fronts beyond distances of the order of the size of the local acoustic disturbance, a function of the laser beam spot size. $\Omega_f(z)$ represents the inverse of the transit time at each distance z along the axis required for acoustic energy in the fluid to cross the spatially broadened source aperture. Using the free and rigid boundary components of the FT of the pressure signal, Eqs. (32) and (33) can be modified to take into account diffraction effects in the fluid:

$$p_f(z,\omega) = \frac{I_0 K_s T_{fs}}{c_s(1+r_{as})} f_s(L,\omega) \times [r_{as}\Gamma_{Rs}(\omega) + \Gamma_{Fs}(\omega)] g_f(\omega) \exp(-ik_{0f}z). \quad (40)$$

C. Time-Domain Photothermoacoustic Pressure Waves

Assuming pulsed excitation of the structure in Fig. 1 of arbitrary temporal profile $I_0 F_P(t)$, with Fourier transform $I_0 f_P(\omega)$, the FT of the generated temperature field is given by

$$\vartheta_s(z,\omega) = -\left(\frac{iI_0\mu_s}{\omega\rho_s C_{sP}}\right) f_P(\omega) \exp[-\mu_s(L+z)] \quad (41)$$

instead of Eq. (13). Under this excitation pulse, Eq. (40) that represents the Fourier spectrum of the PTA pressure wave in the fluid must be multiplied by $f_P(\omega)$. When inverted, this yields the time-dependent PTA pressure wave

$$P_f(z,t) = \frac{I_0 K_s T_{fs}}{c_s(1+r_{as})} \left[r_{as} \int_{-\infty}^{\infty} \Gamma_{Rs}(\omega) f_s(L,\omega) f_P(\omega) g_f(\omega) \exp(i\omega\tau) \mathrm{d}\omega + \int_{-\infty}^{\infty} \Gamma_{Fs}(\omega) f_s(L,\omega) f_P(\omega) g_f(\omega) \exp(i\omega\tau) \mathrm{d}\omega \right], \quad (42)$$

where $\tau = t - (z/c_{0f})$ is a retarded time measured from the fluid origin (the solid–fluid interface). Considering Eqs. (33) for $p_f^{(R)}(z,\omega)$ and $p_f^{(F)}(z,\omega)$ for the weighted components of the pressure wave, we can identify the first and second term under the integral signs on the right-hand side of Eq. (42) with the inverse FT of these two quantities as the time-dependent pressure spectral component under rigid boundary conditions $P_f^{(R)}(z,\tau)$ and under free boundary conditions $P_f^{(F)}(z,\tau)$, respectively. It is easy to verify that the following relation exists between these two components:

$$P_f^{(F)}(z,\tau) = \left(\frac{1}{r_{as}\mu_s c_s}\right) \frac{\mathrm{d}}{\mathrm{d}\tau} P_f^{(R)}(z,\tau). \quad (43)$$

This relationship indicates that, for any shape of the laser pulse, the line shape of the PTA response in a free boundary configuration is the derivative with respect to the retarded time of the line shape of the PTA response in a rigid boundary configuration. This is the mixed-boundary-condition generalization of a similar relation derived by Burmistrova *et al.*[13] Inserting Eq. (34) into Eq. (42), it can be shown that the infinite set of pulse interreflections at the two interfaces of the solid layer will appear at any arbitrary position z in the fluid at delay times defined by

$$\tau_n(z) = t - \frac{z}{c_{0f}} - (2n+1)\frac{L}{c_s}, \quad n = 0,1,2,\ldots, \quad (44)$$

where the origin of times is the onset of the laser pulse. In the special case of the first transmitted pressure pulse across the solid–fluid boundary, $n=0$, the PTA diffraction response in the fluid [Eq. (33a)] can be simplified as follows:

$$P_f^{(R)}(z,\tau_0) = \frac{I_0 K_s T_{fs}}{c_s}\left(\frac{r_{as}}{1+r_{as}}\right)\int_{-\infty}^{\infty}\Gamma_{Rs}(\omega)g_f(\omega)\exp(i\omega\tau_0)\mathrm{d}\omega. \tag{45}$$

The respective diffractionless PTA response is simply given by

$$P_{0f}^{(R)}(z,\tau_0) = \frac{I_0 K_s T_{fs}}{c_s}\left(\frac{r_{as}}{1+r_{as}}\right)\int_{-\infty}^{\infty}\Gamma_{Rs}(\omega)\exp(i\omega\tau_0)\mathrm{d}\omega. \tag{46}$$

Let us invoke the convolution theorem and note that

$$\mathrm{FT}^{-1}[g_f(z,\omega)] = G_f(z,t) = 2\pi\{\delta(t) - \Omega_f(z)\exp[-\Omega_f(z)t]H(t)\}, \tag{47}$$

where $H(t)$ is the Heaviside function and $\delta(t)$ is the Dirac delta function. Using Eqs. (29) and (30) we find from Eqs. (45) and (46)

$$P_f^{(R)}(z,\tau_0) = \mu_s c_s r_{as}\int_{-\infty}^{\infty}P_{0f}^{(F)}(z,t')\exp[-\Omega_f(z)(\tau_0 - t')]\mathrm{d}t'. \tag{48}$$

This convolution formula is a generalization of a relation derived by Terzic and Sigrist[16] for a semi-infinite optically absorbing fluid layer without the presence of a solid overlayer. The same relationship can be found for all subsequent reflection pulses in the present geometry by replacing τ_0 with τ_n. Terzic and Sigrist, however, found different exponent coefficients $\Omega_f(z)$ for direct optical incidence on opaque and transparent fluids,[16,17] representing the single-layer fluid configuration.

D. Viscosity Effects

When Eq. (15) for the FT of the one-dimensional velocity potential is modified to allow for viscous effects in Eq. (4), the resulting Helmholtz equation can be written as

$$\frac{\mathrm{d}^2}{\mathrm{d}z^2}\psi_f(z,\omega) + k_{bf}^2\psi_f(z,\omega) = 0, \quad 0 \leqslant z < \infty, \tag{49}$$

where the viscous wave number in the fluid, k_{bf}, is a complex quantity:

$$k_{bf}^2 = \frac{k_{0f}^2}{1+i\nu_b}, \quad \nu_b \equiv \frac{k_{0f}b}{\rho_f c_{0f}}. \tag{50}$$

Here b is the total fluid viscosity (bulk and shear). The effects of viscosity can be straightforwardly incorporated in the PTA pressure-wave formalism by simply substituting k_{bf} for k_{0f} in all relevant spectral equations. The complex nature of the viscous wave number implies spatial amplitude attenuation of the Fourier component of the propagating wave in the form

$$\exp(-ik_{bf}z) = \exp[-k_{0f}(z/z_A)\sin(\theta/2)] \times \exp[-ik_{0f}(z/z_A)\cos(\theta/2)], \tag{51}$$

where $\theta = \tan^{-1}(\nu_b)$ is a loss angle characterizing the disappearance of mechanical energy from the photomechanical system through conversion in the form of thermal friction. The characteristic damping distance z_A is defined as

$$z_A = (1+\nu_b^2)^{1/2}/k_{0f}. \tag{52}$$

3. EXPERIMENTAL CONFIGURATION AND COMPUTATIONAL IMPLEMENTATION OF THE THEORY

The experimental setup used for our tests is shown in Fig. 2. The laser used to generate PTA pressure waves was a *Q*-switched Nd:YAG laser (Quantel, 1064 nm, 5-ns pulse width, beam size 5–6 mm in diameter). A 45-deg high-energy flat reflection mirror was used to direct the laser beam to the target. A focusing lens was used to change the beam size as required at the target so as to ensure the one dimensionality of the PTA response. Black conical polystyrene target wells were filled with purified water. The inside diameter of the target was 7.10 ± 0.15 mm (top) tapered down to 6.4 ± 0.15 mm (bottom). The nominal base thickness of the black polystyrene wells varied from 1.1 to 1.4 mm. Two membrane needle hydrophones (Models 2312 and 2313, Force Technology, Brøndby, Denmark) with a 1-mm-diameter sensitive element were used depending on laser fluence. The hydrophone was positioned along the axis of the cylindrical well at different depths to measure the pressure-wave pulses. The hydrophones were calibrated up to 20 MHz. The detected signals were displayed on a fast digital oscilloscope (Tektronix, Model 3302). The pressure-wave pulses were captured by the single sequence mode, and the oscilloscope was triggered by the pressure-wave pulse itself. Each waveform was obtained up to three times and stored for statistical purposes, but waveforms from a single target were not averaged because of base ablation. The energy of the Nd:YAG laser could be varied in the range of 60–365 mJ. All experiments took place at room temperature. The hydrophone transfer function was obtained from the manufacturer and was used to determine the frequency-domain roll-off and the time-domain broadening of the PTA impulse response of an essentially delta function laser pulse (~5 ns) on the time scale of the acoustic response (of the order of microseconds). We calculated the absolute pressure at the peak of the response from the hydrophone manufacturer's data using a table of conversion factors (volts per pascal) for each frequency component of the signal and an instrumental sensitivity correction factor to multiply each spectral component of Eq. (42) before the inverse Fourier transformation in the time domain.

Computational implementation of the PTA pressure theory [Eq. (42)] was partly guided by the observed re-

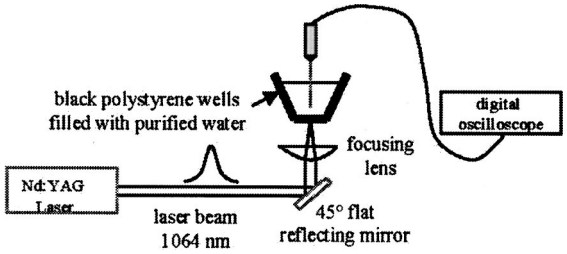

Fig. 2. Experimental setup of our laser PTA drug delivery system.

sults and was separated into a system transfer function factor and a fluid pressure response factor. System transfer function factors were the effect of the solid target $f_s(L,\omega)$; the effect of diffraction in water $g_f(\omega)$; and the effect of the hydrophone response and the spectrum of input pulse waveform, both grouped together in $f_p(\omega)$. The intrasolid reflections are computationally a modification of the first (directly transmitted) impulse response of the solid into the fluid, appropriately time shifted by $\Delta\tau_n = 2n(L/c_s)$ [Eq. (44)] and scaled by the reflectance product $R_{fs}R_{as}$ for each full reflection. The inverse Fourier transform was first calculated with $f_p(\omega)=1$ representing the impulse response of the solid–liquid geometry corresponding to an infinitely narrow laser pulse (mathematically a Dirac delta function). The actual response in the time domain was then considered as a convolution of this with the product of the input pulse and the numerical hydrophone transfer function $f_p(\omega)$. But for some constant multiplication factors, multiplying the diffraction transfer function [Eq. (39)] by $[r_{as}\Gamma_{rs}(\omega)+\Gamma_{fs}(\omega)]$ gives the total system transfer function for the first direct pressure-pulse transmission across the solid–fluid boundary. Taking the inverse Fourier transform of the total system transfer function gives the impulse response in the time domain as

$$h_f(\tau) = \frac{1}{2}c_s\mu_s(1+r_{as})\left[\left(\frac{1}{1+B}\right)\exp(c_s\mu_s\tau)H(-\tau) - \left(\frac{R_{as}}{1-B}\right)\exp(-c_s\mu_s\tau)H(\tau)\right] + \frac{c_s\mu_s B(B-r_{as})}{1-B^2}\exp(-c_s\mu_s B\tau)H(\tau), \quad (53)$$

where $B(z)\equiv 2(c_{0f}z/c_s\mu_s W^2)$ and τ is the retarded time. Since the system impulse response is known, then the PTA response to any given input pulse signal can be found by convolving the input pulse with the impulse response. Assuming an arbitrary input photoacoustic pulse $I_0F_P(t)$ that satisfies $F_P(t)=0$ for $t\leqslant 0$, it can be shown that the total system response is given by

$$P_f(z,\tau) = I_0C_1f_1(0)\exp(c_s\mu_s\tau)H(-\tau) + I_0[C_1\exp(c_s\mu_s\tau)f_1(\tau) - C_2\exp(-c_s\mu_s\tau)f_2(\tau) + C_3\exp(-c_s\mu_s B\tau)f_3(\tau)]H(\tau), \quad (54)$$

where

$$f_1(\tau) = \int_\tau^\infty F_P(t)\exp(-c_s\mu_s t)\mathrm{d}t, \quad (55a)$$

$$f_2(\tau) = \int_0^\tau F_P(t)\exp(c_s\mu_s t)\mathrm{d}t, \quad (55b)$$

$$f_3(\tau) = \int_0^\tau F_P(t)\exp(c_s\mu_s Bt)\mathrm{d}t. \quad (55c)$$

The remaining constants in Eq. (53) are defined as

$$C_1 = \frac{c_s\mu_s(1+r_{as})}{2(1+B)}, \quad C_2 = \frac{c_s\mu_s(1+r_{as})R_{as}}{2(1-B)}, \quad C_3 = \frac{c_s\mu_s B(B-r_{as})}{(1-B^2)}. \quad (55d)$$

As discussed above, the nonlinear frequency response of the hydrophone and its high-frequency roll-off was responsible for the significant broadening of the acoustic signal (>1 μs) compared to the actual laser pulse width. This type of broadened pressure pulse width observed in our experiments has also been reported by authors who used similar hydrophone polyvinylidene fluoride (PVDF) detection schemes with up to a few ($\sim$10) megahertz response.[4] On the other hand, when broadband, 9-μm-thick PVDF transducers were used, the temporal resolution of pressure waveforms achieved was of the order of a few nanoseconds, both in the literature[1] as well as in our system; however, the sensitivities of the PVDF transducer and the signal-to-noise ratio were too compromised compared with the hydrophone transducers to yield good parametric measurements, so we finally opted for the latter. For computational analysis purposes in this study, the convoluted temporal pulse shape of the transducer acting as a low-pass filter was taken as $F_P(t)$ and fitted to a numerical functional form, an extension of the temporal shape best fit reported by Terzic and Sigrist[16]:

$$F_P(t) = \left\{A_1\left(\frac{t}{\tau_R}\right)^2\exp[-A_2(t/\tau_R)] + A_3\left(\frac{t}{\tau_R}\right)^3\exp[-A_4(t/\tau_R)]\right\}H(t). \quad (56)$$

Given a convenient form for $F_P(t)$ such as the one above, then $P_f(z,\tau)$ can be found in closed form with symbolic mathematics software such as MAPLE. Once the analytical form for $P_f(z,\tau)$ is known, it can be used to fit the experimental data. Here (A_1–A_4) are constants determined by fitting to the frequency response data of the manufacturer-supplied hydrophone transducer upon inverse FT to the time domain, as is τ_R, a parameter representing the laser plus transducer (instrumental) rise time. We found that this method of mathematically describing the transient excitation waveform empirically and using it in the convolution of the theoretical PTA response obtained from the experimental data proved to be faster and more effective than purely numerical integration or time-domain convolution schemes.[7,15]

4. EXPERIMENTAL RESULTS, COMPUTATIONAL FITS TO DATA, AND DISCUSSION

Figures 3–14 show experimental PTA results under various laser intensity and hydrophone location conditions. To obtain best fits to the entire time record of the pressure responses, the exact values of A_1–A_4 were not as important as the value of τ_R in Eq. (56). Overall, the important fitting factors are (i) the product $\zeta_s = c_s\mu_s$ of the optical absorption coefficient and the speed of sound in the solid, (ii)

the fluid diffraction parameter $B(z)$, (iii) the acoustic impedance coefficient at the air–solid boundary r_{as}, and (iv) the effective instrumental excitation width τ_R. With regard to r_{as}, it is interesting to note that increasing the gas–solid acoustic impedance term r_{as} in Eq. (28) increases the pressure magnitude, since more energy is confined in the region $z > -L$ (Fig. 1). This term is affected when a variable acoustic impedance layer is added to the solid–air interface before exposure to laser pulses. Such surface loading laser ultrasonic effects have been observed experimentally in our experiments (when we use a thin layer of gel) and also previously by a number of authors. They have been reviewed in some detail by Hutchins.[18] We selected the reported results in this work among waveform data obtained using either the Force hydrophone transducer Model 2312 (low pulse energies of 60 and 100 mJ) or Model 2313 (high pulse energies of 165 and 265 mJ). These particular sets of data were chosen so as to show the trends in goodness of fit as a function of incident pulse energy, among other measurements. This, is turn, is insightful regarding the onset of nonlinear photothermoelastically driven hydrodynamic behavior in the system. All data figures include experimental pressure-wave traces and superposed theoretical best fits. The parameters used for the theoretical fits are $\rho_a = 1.293\ \mathrm{kg/m^3}$, $c_a(20\,^\circ\mathrm{C}) = 344\ \mathrm{m/s}$, $\rho_f = 998\ \mathrm{kg/m^3}$, $c_{0f} = 1481\ \mathrm{m/s}$, $W = 5.5\ \mathrm{mm}$, and $\beta_T = 0.8 \times 10^{-4}/^\circ\mathrm{C}$.[19] Viscous damping in the form of a complex wave number k_{bf} [Eq. (50)] was first introduced into the computational fitting procedure, but it was found that all theoretical fits in this work were able to be accommodated with no viscous damping.

In Fig. 3 data from the 60-mJ laser pulse are shown, with the transducer located at $z = 2$ mm away from the solid polystyrene target bottom (the well). The bipolar pulse width (compression peak followed by the rarefaction trough) is fitted well for both primary (i.e., early) response and secondary response (first reflection, following a round trip of acoustic energy in the solid target). The temporal delay between the primary and the reflected pulses determines precisely the thickness of the bottom of the well,

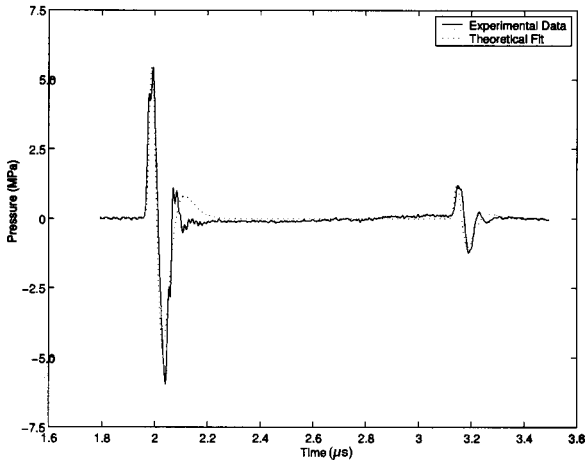

Fig. 3. Experimental PTA data and theoretical fit for laser-pulse energy of 60 mJ and an axial hydrophone distance $z = 2$ mm. The fit parameters are $B = 0.162$, $c_s\mu_s = 2.2 \times 10^8\ \mathrm{s^{-1}}$, $L = 1.27 \times 10^{-3}$ m, $r_{as} = 1.86 \times 10^{-4}$, $\tau_R = 9.52 \times 10^{-8}$ s.

assuming the speed of sound in polystyrene to be $c_s = 2358$ m/s (an average between values reported in the literature[4,20]). The various fitted parameters, including the optimal thickness L of the well bottom, are shown in the caption of Fig. 3. Nominal thickness L was in the 1.1–1.4-mm range. The secondary pressure compression (third extremum in the fundamental tripolar pulse) is not fitted well in Fig. 3. This relatively sharp peak and similar peaks in subsequent plots are not accounted for in our theory. Satellite experiments over longer time scales that used a series of laser irradiances showed that the rapid damped oscillations following the primary photoacoustic pulse and its first reflection were due to transducer ringing with a period $\sim 0.1\ \mu$s. Similar photoacoustic ringing effects have been reported by Sigrist.[15] We attempted to eliminate these resonances mathematically by multiplying the PTA response expression of Eq. (42) with the FT of a simple damped harmonic-oscillator model of the form

$$f_m(t) = A_m \exp(-t/\tau_m)\cos(\omega_m t + \phi_m), \quad t \geqslant 0. \tag{57}$$

Quantities with the subscript m denote values at resonance. The transducer transfer function in the frequency domain consists of two contributions at $\omega_\pm = \omega \pm \omega_m$:

$$F_m(\omega) = \frac{A_m \tau_m}{4\pi}\left[\frac{\exp(-i\phi_m)}{1 + i\omega_t + \tau_m} + \frac{\exp(i\phi_m)}{1 + i\omega_t - \tau_m}\right]. \tag{58}$$

Unfortunately, the high-frequency background noise rendered the precise identification of the resonance frequency ω_m difficult from experiment to experiment with peak-to-peak variations as large as 0.05 μs, which significantly reduced the utility of the mathematical elimination procedure as it tended to distort the temporal position of the diffraction peaks. Therefore the attempt was abandoned, and pressure transients were used as obtained. Here, the best fit consisted of matching the curvature of the structure at the foot of the experimental ringing peak, which is most likely due to diffraction. It can be argued that the experimental pulse shape between 2.0 and 2.2 μs is the superposition of diffraction and transducer resonant ringing.

Figure 4 shows similar curves at hydrophone position $z = 5$ mm. Here again, the fundamental compression and rarefaction (bipolar) waveform zone is well fitted with the first resonant ringing of the transducer occuring $\sim 0.14\ \mu$s after the onset of the PTA pulse. The best-fitted theoretical second (diffraction) maxima of both primary and reflected pulses are delayed with respect to the resonant peak that precedes the theoretical maximum. The same trend occurs in Fig. 5 obtained with the hydrophone position at $z = 8$ mm. The degree of waveform reproducibility from shot to shot was calculated in terms of the temporal position of the various PTA extrema for pressure-pulse traces from three wells at each location of the hydrophone as follows: 0.11 μs or ±1.05% for $z = 2$ mm, 0.13 μs or ±1.2% for $z = 5$ mm, and 0.16 μs or ±1.6% for $z = 8$ m. Similar reproducibility tolerances were measured with all other laser fluences (Fig. 15). It can be seen in Fig. 5 that the experimental trough (negative peak) of the fundamental bipolar rarefaction begins to trail the compression peak very slightly at farther locations of the hydrophone compared with $z = 2$ mm. This is also clear from the theo-

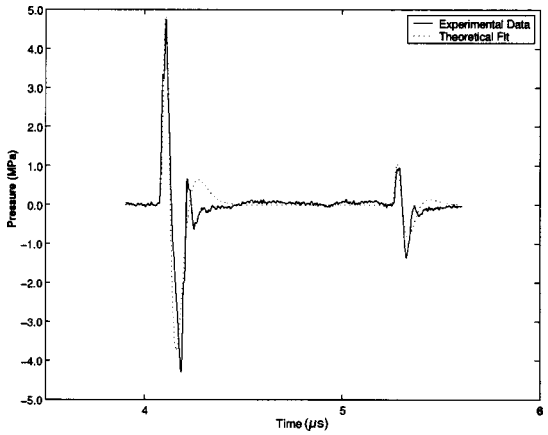

Fig. 4. Experimental PTA data and theoretical fit for a laser-pulse energy of 60 mJ and an axial hydrophone distance $z=5$ mm. The fit parameters are $B=0.404$, $c_s\mu_s=2.2\times10^8$ s^{-1}, $L=1.30\times10^{-3}$ m, $r_{as}=1.86\times10^{-4}$, $\tau_R=8.76\times10^{-8}$ s.

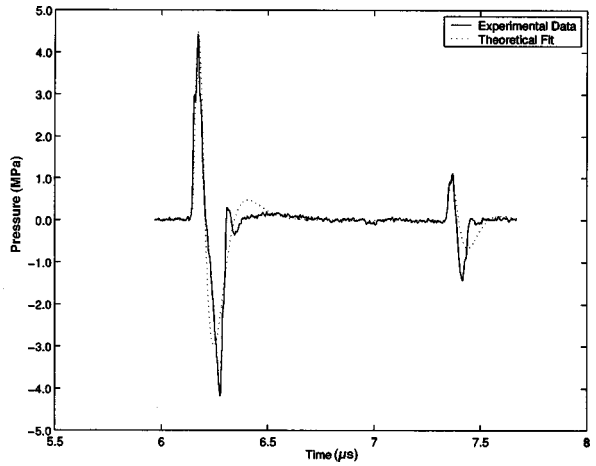

Fig. 5. Experimental PTA data and theoretical fit for a laser-pulse energy of 60 mJ and an axial hydrophone distance $z=8$ mm. The fit parameters are $B=0.646$, $c_s\mu_s=2.2\times10^8$ s^{-1}, $L=1.31\times10^{-3}$ m, $r_{as}=1.86\times10^{-4}$, $\tau_R=8.90\times10^{-8}$ s.

retical fits. It is thus concluded[21] that, even at these very low laser-pulse energies, this trend is consistent with the onset of hydrodynamic nonlinearity in water. From Figs. 3–5, in this almost purely linear hydrodynamic region, the best-fitted values of $B=B(z)$ increase essentially linearly with z, as predicted by the definition of B in Eq. (53) and Ref. 17. The best-fitted value of B for each transient is mostly sensitive to the temporal difference between the primary compression and the rarefaction peaks. An optimal compromise to best fit both the primary and the reflected traces had to be made in all cases with the reported values reflecting this compromise.

For laser-pulse energy of 100 mJ, Fig. 6 shows the $z=2$-mm data. Again, the primary compression and rarefaction peaks are fitted well, with the exception of the secondary maximum (sharp peak) due to the transducer resonance that occurs at ~0.16 μs after the onset of the PTA pulse and is much reduced with respect to the 60 -mJ case because of the increased absolute PTA signal (pressure peak) level. This fact has allowed a better fit of the tripolar wave to (minimal) diffraction effects at both the primary and the first reflection pulses. Figure 7 is the hydrophone response at $z=5$ mm. The response peak amplitude is significantly weaker than at $z=2$ mm because of the more remote location of the transducer with respect to the source. Thus the resonance effect following the rarefaction trough appears enhanced, to the detriment of a good diffraction fit to the primary tripolar response. The diffraction fit to the first reflection pulse, however, is much improved because of resonance damping at longer times, and the diffraction parameter B is larger than that at the $z=2$-mm position, as expected [Eq. (53) and Ref. 17].

Figure 8 shows the 100-mJ results at $z=8$ mm. Here the diffraction peak of the fundamental tripolar wave is improved, trailing behind the resonance peak following the rarefaction trough. The best-fitted value of $B(z)$ follows the expected increasing trend with increasing transducer distance from the point of the PTA disturbance; however, the primary theoretical trough minimum trails behind the experimental minimum. This is due to the onset of measurable nonlinearity of the response at the far

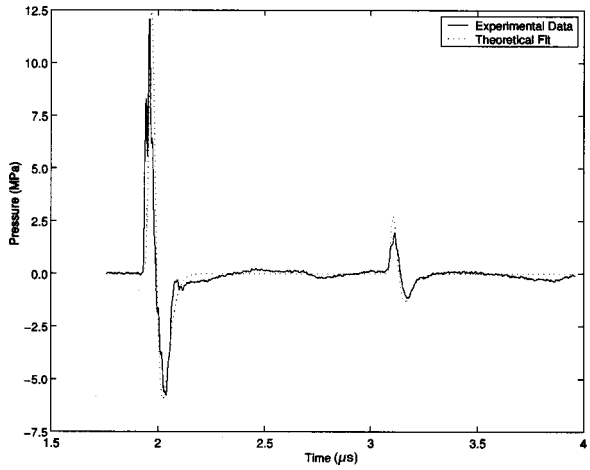

Fig. 6. Experimental PTA data and theoretical fit for a laser-pulse energy of 100 mJ and an axial hydrophone distance $z=2$ mm. The fit parameters are $B=0.011$, $c_s\mu_s=2.2\times10^8$ s^{-1}, $L=1.25\times10^{-3}$ m, $r_{as}=1.86\times10^{-4}$, $\tau_R=8.76\times10^{-8}$ s.

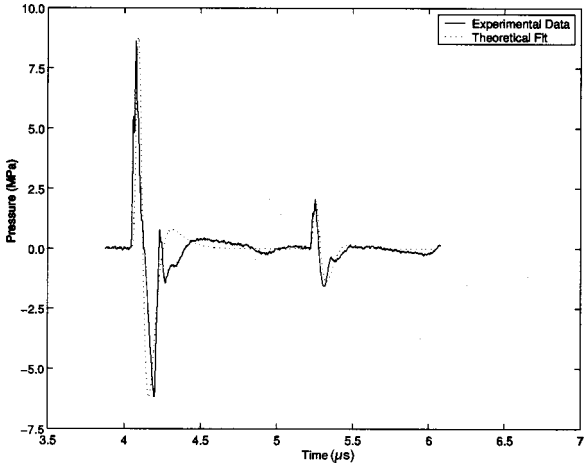

Fig. 7. Experimental PTA data and theoretical fit for a laser-pulse energy of 100 mJ and an axial hydrophone distance $z=5$ mm. The fit parameters are $B=0.043$, $c_s\mu_s=2.2\times10^8$ s^{-1}, $L=1.28\times10^{-3}$ m, $r_{as}=1.86\times10^{-4}$, $\tau_R=8.90\times10^{-8}$ s.

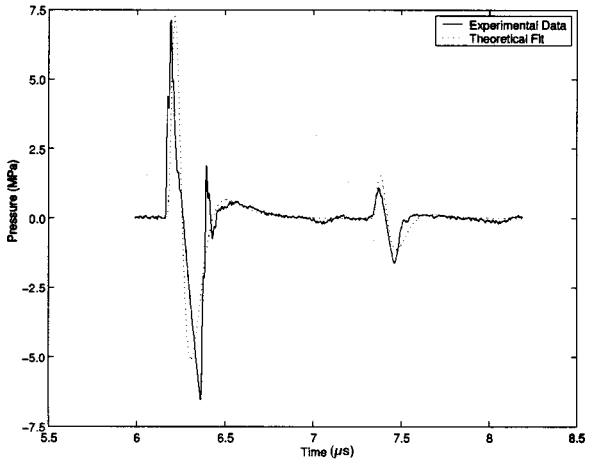

Fig. 8. Experimental PTA data and theoretical fit for a laser-pulse energy of 100 mJ and an axial hydrophone distance $z=8$ mm. The fit parameters are $B=0.069$, $c_s\mu_s=2.2\times10^8$ s^{-1}, $L=1.28\times10^{-3}$ m, $r_{as}=1.86\times10^{-4}$, $\tau_R=9.02\times10^{-8}$ s.

location of the hydrophone; it is cumulative in time and manifests itself as a higher speed of propagation of sound in the water, thus steepening the rising edge of both the primary and the first reflection pressure pulses as predicted theoretically.[7,21] The lower B values at 100-mJ pulse energy compared with the 60-mJ fits cannot be explained in a straightforward manner within the confines of the present linear PTA theory. It is strongly suspected, however, that the visually observable target surface scorching after each laser pulse that appears at 100 mJ and higher energies is probably responsible for the onset of nonlinear ablation effects on the polystyrene in the range of photoacoustic pressures ($\sim$5–10 MPa) that arise in the 100-mJ and higher pulse energy experiments. Ablation is expected to affect (increase) the speed of sound c_s in the solid itself or increase the optical absorption coefficient μ_s of the polystyrene surface thus decreasing the absolute value of B since $B\propto 1/c_s\mu_s$. Surface ablation has been observed in polyimide targets in the same peak pressure range[22] and has resulted in a sublinear laser photoacoustic response on a plot of peak pressure (stress) versus laser fluence. This type of sublinear behavior was also present in our measurements (Fig. 15). Shot-to-shot reproducibility over three transients is indicated by the error bars in Fig. 15. Each transient was obtained with a different polystyrene target so as to avoid the effects of multiple pulse ablation on one target.

In the results with a laser-pulse energy of 165 mJ, Figs. 9–11, the peak-to-trough ratio decreases with increasing hydrophone distance from the bottom of the well. The bump at the trailing foot of the primary compression peak is the first transducer resonance and occurs at $\sim$0.14 μs ($z=2$ mm) and $\sim$0.23 μs ($z=5$ mm) following the onset of the laser pulse. It clearly prevents the full formation of the rarefaction trough at $z=2$ and 5 mm. The same resonant feature also appears, albeit significantly damped, after the first reflection peak. The farthest positioning of the hydrophone at $z=8$ mm shows a well-pronounced shift of the fundamental rarefaction trough followed by steepening of the rising edge of the secondary maximum of the tripolar pulse. The goodness of fit to the first reflection trough is due to the damping of the resonance peak under the much stronger PTA pressure pulse and is probably accidental as it involves nonlinear distortions not accounted for in the present linear PTA theory. It is clear that nonlinearity due to polystyrene material ablation (see the strong sublinear behavior at $z=8$ mm in Fig. 15) significantly distorts the rarefaction trough, thus also distorting the best-fitted value of the diffraction parameter B at that feature away from its monotonically increasing behavior compared with closer locations of the transducer (Fig. 11).

Finally, for laser-pulse energies of 265 mJ (Fig. 12), it is clear that nonlinear effects essentially dominate the PTA fundamental tripolar pressure compression wave, with transducer ringing distorting the full formation of the rarefaction trough at the hydrophone position $z=2$ mm. The strong resonance effect at $z=2$ mm is most likely due to the intense photoacoustic-induced ringing at high fluid pressures ($\geqslant$15 MPa). The combination of higher laser irradiance and longer distance of the transducer from the PTA pulse generation in the cases of $z=5$ and 8 mm ap-

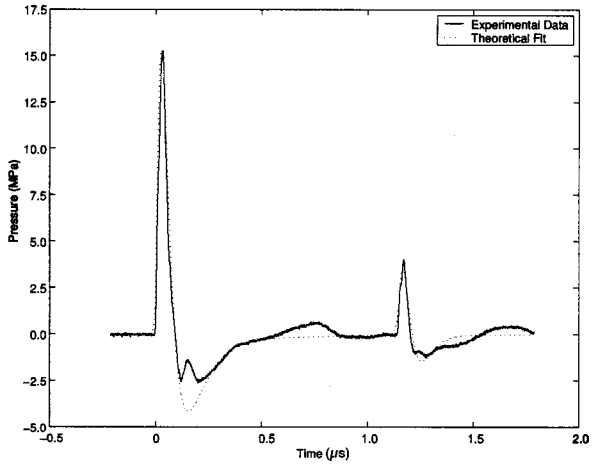

Fig. 9. Experimental PTA data and theoretical fit for a laser-pulse energy of 165 mJ and an axial hydrophone distance $z=2$ mm. The fit parameters are $B=0.022$, $c_s\mu_s=1.98\times10^8$ s^{-1}, $L=1.35\times10^{-3}$ m, $r_{as}=1.73\times10^{-4}$, $\tau_R=1.05\times10^{-7}$ s.

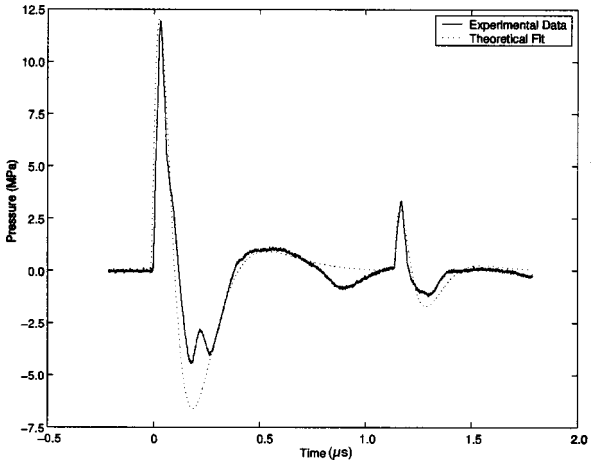

Fig. 10. Experimental PTA data and theoretical fit for a laser-pulse energy of 165 mJ and an axial hydrophone distance $z=5$ mm. The fit parameters are $B=0.036$, $c_s\mu_s=3.17\times10^8$ s^{-1}, $L=1.35\times10^{-3}$ m, $r_{as}=1.73\times10^{-4}$, $\tau_R=9.02\times10^{-8}$ s.

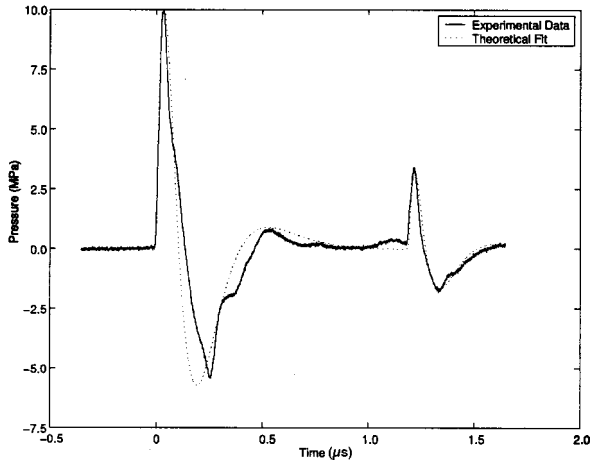

Fig. 11. Experimental PTA data and theoretical fit for a laser-pulse energy of 165 mJ and an axial hydrophone distance $z=8$ mm. The fit parameters are $B=0.006$, $c_s\mu_s=1.98\times10^8$ s^{-1}, $L=1.41\times10^{-3}$ m, $r_{as}=1.73\times10^{-4}$, $\tau_R=1.07\times10^{-8}$ s.

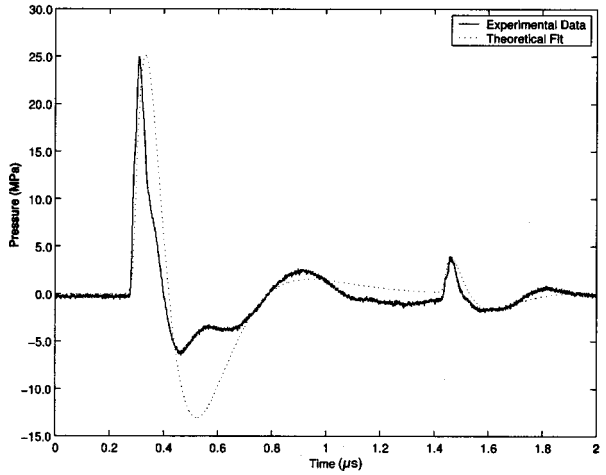

Fig. 12. Experimental PTA data and theoretical fit for a laser-pulse energy of 265 mJ and an axial hydrophone distance $z=2$ mm. The fit parameters are $B=0.094$, $c_s\mu_s=1.54\times10^8$ s^{-1}, $L=1.35\times10^{-3}$ m, $r_{as}=67\times10^{-4}$, $\tau_R=8.93\times10^{-8}$ s.

parently minimizes the contribution of the resonance to the transient in Figs. 13 and 14. The effect on best-fitted $B(z)$ values is to yield nonmonotonic (and thus meaningless) trends in this quantity. Furthermore, the considerable steepening of the fundamental compression wave exhibits an earlier peak than the linear theory predicts at all three transducer locations. When not concealed by the transducer resonance at the more remote hydrophone positions in Figs. 13 and 14, the falling edges of both fundamental and first-reflection compression pulses tend toward the formation of an N-shaped waveform with a sharpened tripolar maximum, characteristic of hydrodynamic nonlinearity superposed on diffraction.[21] This feature amounts to strong evidence that nonlinear acoustics begin to dominate this regime of laser pulses. For the fully nonlinear behavior and perhaps the unipolar pressure pulses reported in similar experiments,[1–4] the present studies show that energy higher than 265 mJ for an unfocused laser pulse is required.

The functional relations between the incident laser pulse (or irradiance) and the generated photoacoustic peak pressure pulse in water are shown in Fig. 15 for three locations of the hydrophone transducer along the symmetry axis of the polystyrene wells. It is clear that the relationship between these quantities is linear in the wave near-field region $z=2$ mm and that it grows progressively nonlinear at more remote locations in the well. The sublinear behavior of the curves is consistent with the predictions of Zweig and Deutsch[23] regarding the stress coupling coefficient for polyimide in the plasma-mediated ablation region. The stress coupling coefficient is defined as the total momentum transfer to the target during ablation divided by the laser-pulse energy.[24] The irradiance range of our experiments, 1.26–5.3 MW/cm^2, is within the plasma ablation regime that was shown to exhibit peak stress σ_p versus laser irradiance I dependence of the form $\sigma_p\propto I^{0.7}$.[23,24] Another possibility for the sublinear PTA pulse behavior at large distances in Fig. 15 is the higher dimensionality of the generated acoustic wave that would tend to distribute acoustic energy in directions other than along the axis of symmetry of the well.[25] The appearance of a higher dimensionality depends on the dif-

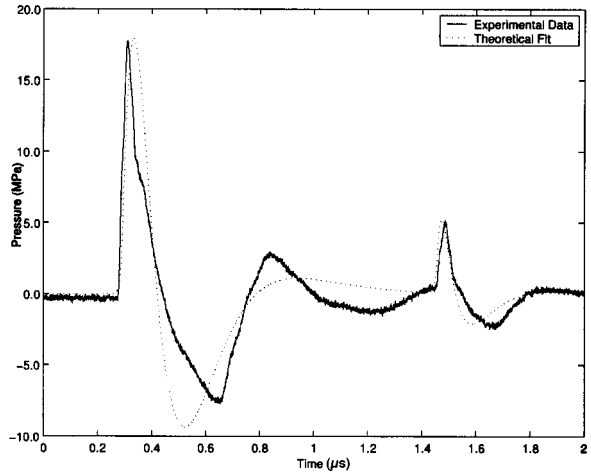

Fig. 13. Experimental PTA data and theoretical fit for a laser-pulse energy of 265 mJ and an axial hydrophone distance $z=5$ mm. The fit parameters are $B=0.047$, $c_s\mu_s=1.54\times10^8$ s^{-1}, $L=1.37\times10^{-3}$ m, $r_{as}=67\times10^{-4}$, $\tau_R=1.07\times10^{-8}$ s.

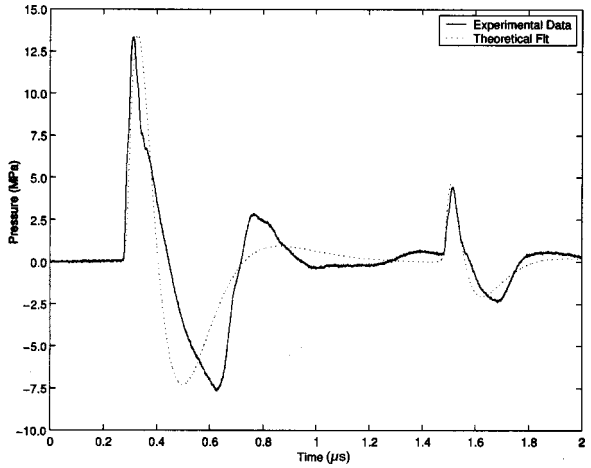

Fig. 14. Experimental PTA data and theoretical fit for a laser-pulse energy of 265 mJ and an axial hydrophone distance $z=8$ mm. The fit parameters are $B=0.076$, $c_s\mu_s=1.54\times10^8$ s^{-1}, $L=1.41\times10^{-3}$ m, $r_{as}=67\times10^{-4}$, $\tau_R=1.0\times10^{-8}$ s.

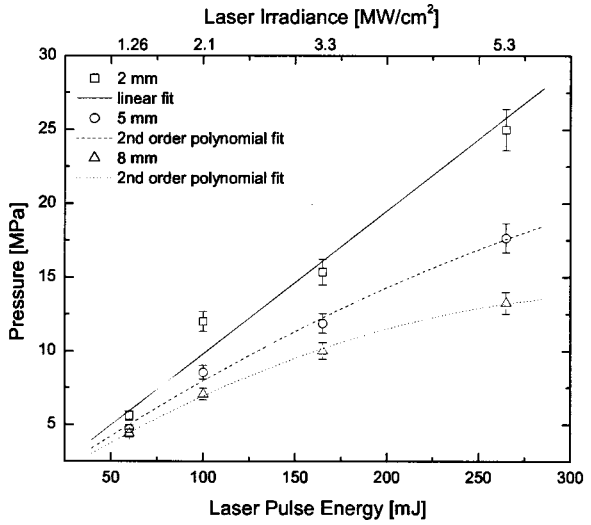

Fig. 15. PTA peak pressure of the primary condensation pulse in water versus incident laser fluence for three locations of the hydrophone. $z=8$ mm (triangles), $z=5$ mm (circles), $z=2$ mm (squares).

fraction length in the fluid. The dominant mechanism for the sublinear behavior is determined by the ratio $L_{\mathrm{DF}}/L_{\mathrm{NL}}$ in the fluid, where L_{NL} is the nonlinearity characteristic length. It can be shown (Ref. 7, Chap. 2.3) that $L_{\mathrm{DF}}/L_{\mathrm{NL}}=\epsilon\omega^2W^2v_a/2c_{0f}{}^3\ll 1$ in water. Here ϵ is the nonlinear acoustic parameter of water [4.4±0.9 (Ref. 6)] and v_a is the amplitude of the particle (vibrational) velocity. In this case nonlinear effects due to ablation are expected to become noticeable only in the far field of the PTA wave, consistent with the trends in Fig. 15, where the degree of nonlinearity increases with increasing distance from the pulse generation point. Theoretically a fully nonlinear model of the coupled solid–fluid hydrodynamic behavior is needed. There are two ways to achieve this with the pulse time records generated in our experiments: either through numerical solution of the so-called Khokhlov–Zabolotskaya equation[26] or through the application of a theorem (in the form of a boundary-value problem) in nonlinear acoustics, known as the Poisson solution.[27] Work toward the implementation of a fully nonlinear PTA theory at large laser fluences is currently under way.

5. CONCLUSIONS

A linear time-domain PTA theory has been developed for a composite solid–liquid one-dimensional geometry that includes multiple interreflections at interfaces, acoustic diffraction effects, and natural mixed boundary conditions at the source interface (air–solid). The theory was applied to experimental laser-induced pressure-wave pulses in a polystyrene well target and water system used for photomechanical drug delivery studies. A computational algorithm based on best fits of the theory to experimental data sets was generated. The results of the fits show the following trends: (1) At low laser-pulse energies $\lesssim$100 mJ, the linear PTA model fits the data well, especially at distances <5 mm from the solid–fluid interface along the axis of symmetry, with the exception of a pressure bump at the secondary rising edge of the primary tripolar pulse, a feature consistent with damped resonant ringing of the transducer. (2) The onset of significant hydrodynamic nonlinearity appears for laser-pulse energies in the 165-mJ range, especially at axial distances $z\geqslant 5$ mm consistent with ablation-induced nonlinearity in the solid polystyrene and transmitted in the underlying water layer. (3) The theoretical fits to the data can be used to measure several geometric, acoustic, optical, and thermodynamic parameters of the experimental system including precise thickness L of the target, its optical absorption coefficient μ_s and any variations due to laser ablation of the surface, its acoustic velocity c_s, the fluid diffraction parameter $B(z)$, and the acoustic impedance r_{as} with and without ablation. The present work can be used to establish the onset of hydrodynamic PTA nonlinearity and control the laser irradiance across the transition region from linearity to optimize the efficiency of photomechanical drug delivery and induce cell permeabilization with laser photomechanical stress waves.

REFERENCES

1. S. E. Mulholland, S. Lee, D. J. McAuliffe, and A. G. Doukas, "cell loading with laser-generated stress waves: the role of the stress gradient," Pharm. Res. **16**, 514–518 (1999).
2. A. G. Doukas, D. J. McAuliffe, S. Lee, V. Venugopalan, and T. J. Flotte, "Physical factors involved in stress-wave-induced cell injury: the effect of stress gradient," Ultrasound Med. Biol. **21**, 961–967 (1995).
3. D. C. Lamb, J. Tribble, A. G. Doukas, T. J. Flotte, R. H. Ossoff, and L. Reunisch, "Custom designed acoustic pulses," J. Biomed. Opt. **4**, 217–223 (1999).
4. T. Kodama, M. R. Hamblin, and A. G. Doukas, "Cytoplasmic molecular delivery with shock waves: importance of impulse," Biophys. J. **79**, 1821–1832 (2000).
5. E. F. Carome, N. A. Clark, and C. E. Moeller, "Generation of acoustic signals in liquids by ruby laser-induced thermal stress transients," Appl. Phys. Lett. **4**, 95–97 (1964).
6. M. W. Sigrist and V. G. Mikhalevich, "New method for nonlinear acoustic studies in liquids using lasers," in *Proceedings of the International Conference on LASERS '82* (STS, New Orleans, La., 1982), pp. 80–85.
7. V. E. Gusev and A. A. Karabutov, *Laser Optoacoustics* (American Institute of Physics, New York, 1993).
8. H. M. Lai and K. Young, "Theory of the pulsed optoacoustic technique," J. Acoust. Soc. Am. **72**, 2000–2007 (1982).
9. L. D. Landau and E. M. Lifshitz, *Fluid Mechanics* (Pergamon, New York, 1959), p. 283. Translation by J. B. Sykes and W. H. Reid.
10. L. E. Kinsler and A. R. Fray, *Fundamentals of Acoustics*, 2nd ed. (Wiley, New York, 1966).
11. W. Nowacki, *Dynamic Problems in Thermoelasticity* (Noordhoff International, Leyden, The Netherlands, 1975).
12. M. I. Khan, T. Sun, and G. J. Diebold, "Photoacoustic waves generated by absorption of laser radiation in optically thin layers," J. Acoust. Soc. Am. **93**, 1417–1425 (1993).
13. L. V. Burmistrova, A. A. Karabutov, A. I. Portyagin, O. V. Rudenko, and E. B. Cherepetskaya, "Method of transfer functions in problems of thermooptical sound generation," Sov. Phys. Acoust. **24**, 369–374 (1978).
14. A. A. Karabutov, A. I. Portyagin, O. V. Rudenko, and E. B. Cherepetskaya, "Experimental study of the propagation of short thermooptically excited acoustic pulses," Sov. Phys. Acoust. **26**, 162–164 (1980).

15. M. W. Sigrist, "Laser generation of acoustic waves in liquids and gases," J. Appl. Phys. **60**, R83–R121 (1986).
16. M. Terzic and M. W. Sigrist, "Pulsed photoacoustic measurements of large optical absorption coefficients," J. Appl. Phys. **67**, 3593–3596 (1990).
17. M. Terzic and M. W. Sigrist, "Diffraction characteristics of laser-induced acoustic waves in liquids," J. Appl. Phys. **56**, 93–95 (1984).
18. D. A. Hutchins, "Ultrasonic generation by pulsed lasers," in *Physical Acoustics* (Academic, New York, 1988), Vol. 18, Chap. 2.4.
19. "Styrene technical data and information sheet," www.cityplastics.com.au/styrene.html.
20. D. R. Lide, *CRC Handbook of Chemistry and Physics* (CRC Press, Boca Raton, Fla.), pp. 14–38.
21. Ya. M. Zhileikin and O. V. Rudenko, "Nonlinear and diffraction transformation of acoustic pulses," Sov. Phys. Acoust. **27**, 200–202 (1981).
22. A. D. Zweig, V. Vanugopalan, and T. F. Deutsch, "Stress generated in polyimide by excimer-laser irradiation," J. Appl. Phys. **74**, 4181–4189 (1993).
23. A. D. Zweig and T. F. Deutsch, "Shock waves generated by confined excimer laser ablation of polyimide," Appl. Phys. B: Photophys. Laser Chem. **4**, 76–82 (1992).
24. A. G. Doukas and T. J. Flotte, "Physical characteristics and biological effects of laser-induced stress waves," Ultrasound Med. Biol. **22**, 151–164 (1996).
25. T. G. Muir, C. R. Culbertson, and J. R. Clynch, "Experiments on thermoacoustic arrays with laser excitation," J. Acoust. Soc. Am. **59**, 735–743 (1976).
26. N. S. Bakhvalov, Ya. M. Zhileykin, and E. A. Zabolotskaya, *Nonlinear Theory of Acoustic Beams* (Nauka, Moscow, 1982).
27. M. F. Hamilton and C. L. Morfey, "Model equations," in *Nonlinear Acoustics*, M. F. Hamilton and D. T. Blackstock, eds. (Academic, New York, 1998), Chap. 3, pp. 41–63.